

# Soft Matter

Accepted Manuscript



This is an *Accepted Manuscript*, which has been through the Royal Society of Chemistry peer review process and has been accepted for publication.

*Accepted Manuscripts* are published online shortly after acceptance, before technical editing, formatting and proof reading. Using this free service, authors can make their results available to the community, in citable form, before we publish the edited article. We will replace this *Accepted Manuscript* with the edited and formatted *Advance Article* as soon as it is available.

You can find more information about *Accepted Manuscripts* in the [Information for Authors](#).

Please note that technical editing may introduce minor changes to the text and/or graphics, which may alter content. The journal's standard [Terms & Conditions](#) and the [Ethical guidelines](#) still apply. In no event shall the Royal Society of Chemistry be held responsible for any errors or omissions in this *Accepted Manuscript* or any consequences arising from the use of any information it contains.



# In situ dispersion of nonaqueous Fe<sub>3</sub>O<sub>4</sub> nanocolloids by microdroplet coalescence and their use in the preparation of magnetic composite particles

Received 00th January 20xx,  
Accepted 00th January 20xx

DOI: 10.1039/x0xx00000x

www.rsc.org/

Le Du,<sup>a</sup> Yujun Wang,<sup>b</sup> Jianhong Xu,<sup>b</sup> Chun Shen,<sup>\*c</sup> and Guangsheng Luo<sup>\*b</sup>

Monodispersity and size uniformity are critical issues for nanoparticles, especially for the inorganic particles dispersed in organic carriers serving as the precursor of composites. Herein, for the first time, we have developed a method based on flow-induced droplet coalescence for in situ dispersion of surface-modified Fe<sub>3</sub>O<sub>4</sub> nanoparticles to prepare Fe<sub>3</sub>O<sub>4</sub>/polystyrene (Fe<sub>3</sub>O<sub>4</sub>/PS) composite particles. A plate-type microchannel was constructed to initiate droplet coalescence for reducing the water–oil interfacial area and dispersing Fe<sub>3</sub>O<sub>4</sub> nanoparticles into the precursor suspensions. Under optimized conditions, the precursor suspensions could be composed of monodispersed Fe<sub>3</sub>O<sub>4</sub> nanoparticles with an average size of approximately 12 nm. In this case, the saturation magnetization of the prepared superparamagnetic composites was as high as 4.012 emu/g at a magnetite content of 5 wt %. The method is simple and has great potential to be tailored to the preparation of nonaqueous suspensions with uniform and monodispersed nanoparticles.

## 1. Introduction

Coalescence of microdroplets plays an important role in numerous industrial processes such as liquid–liquid extraction, demulsification, and polymer blending.<sup>1–3</sup> In the past two decades, significant attention has been directed towards the flow-induced droplet coalescence with the development of microfluidic technologies, which offer several important advantages for geometric confinement and droplet collision.<sup>4–6</sup> These advantages have been widely exploited in applications such as protein crystallization, cell classification, and other types of bioanalysis.<sup>7–10</sup>

Theoretically, flow-induced droplet coalescence is favorable for in situ dispersion of surface-modified inorganic nanoparticles, which have been increasingly used in the form of organic nanosuspensions during their preparation in two-phase (w/o) systems. The difficulty is due to the interphase mass transfer of surface-modified nanoparticles from the aqueous phase to the organic phase.<sup>11,12</sup> During this process, a number of microdroplets (1–1000 μm) are generated, causing the particles to gather at the phase interface to reduce the

high interfacial energy.<sup>13,14</sup> Upon the introduction of flow-induced coalescence, demulsification could be efficiently performed and the hydrophobic nanoparticles could also be directly transferred into the oil phase, along with the avoidance of undesirable agglomeration.<sup>15,16</sup> However, up to now there have been no investigations on the in situ dispersion of surface-modified nanoparticles based on droplet coalescence, not to mention the preparation of high-concentration nanosuspensions with in situ dispersed particles and their downstream applications.

Recently, with the advances in magnetic organic–inorganic composites, surface-modified inorganic nanoparticles have been extensively investigated due to their ability to adequately disperse into organic solutions, serving as precursor suspensions.<sup>17–19</sup> Composite materials with Fe<sub>3</sub>O<sub>4</sub> nanoparticles are to be of use in solar energy transport, drug delivery, magnetic resonance techniques, and ferrofluids as magnetic resonance materials.<sup>20–22</sup> Especially for the composites with uniformly dispersed Fe<sub>3</sub>O<sub>4</sub> nanoparticles with an average size of less than 20 nm, they can hold paramagnetic or superparamagnetic properties due to the decreased exchange-coupled spins that resist spontaneous reorientation.<sup>23,24</sup> In this case, their strong magnetic properties have rendered them useful with negligible coercivity and remanence.

Several studies have been conducted to prepare Fe<sub>3</sub>O<sub>4</sub> nanosuspensions and Fe<sub>3</sub>O<sub>4</sub>-based composites. For example, Zhao and Nan employed one-pot route to prepare magnetic nanofluids containing Fe<sub>3</sub>O<sub>4</sub>/Polypyrrole nanoparticles by adding FeCl<sub>3</sub> aqueous solution as the iron source into the

<sup>a</sup>The State Key Laboratory of Chemical Resource Engineering, Beijing Key Laboratory of Membrane Science and Technology, Beijing University of Chemical Technology, Beijing 100029, China

<sup>b</sup>The State Key Laboratory of Chemical Engineering, Department of Chemical Engineering, Tsinghua University, Beijing 100084, China. E-mail: gsluo@tsinghua.edu.cn.

<sup>c</sup>Beijing Key Laboratory of Bioprocess, College of Life Science and Technology, Beijing University of Chemical Technology, Beijing 100029, China. E-mail: shenchun@mail.buct.edu.cn.

pyrrole monomer solution.<sup>25</sup> The as-prepared particles exhibited a superparamagnetic behavior for their average size varying in the range of 7–30 nm. Other studies have examined the dynamics of particle transfer in detail, confirming that the dispersion ratio could be significantly increased in the case of simultaneous dispersion.<sup>26,27</sup> In addition to traditional (micro)emulsion methods, a novel technique known as reverse micelle method has been developed, which exhibited better control over the size of magnetic nanoparticles.<sup>28,29</sup> In this case, reverse micelles form microemulsions with a precursor solution where two immiscible liquids coexist. Hydrophobic  $\text{Fe}_3\text{O}_4$  nanoparticles with a size of less than 15 nm could be synthesized by dispersing their precursor into hexane with the presence of oleic acid and oleylamine. Downstream, they were used to prepare magnetic composite particles such as  $\text{Fe}_3\text{O}_4$ /polypropylene ( $\text{Fe}_3\text{O}_4$ /PP),  $\text{Fe}_3\text{O}_4$ /polystyrene ( $\text{Fe}_3\text{O}_4$ /PS),  $\text{Fe}_3\text{O}_4$ /polyurethane ( $\text{Fe}_3\text{O}_4$ /PU), etc.<sup>30–32</sup> However, their saturation magnetization was limited by the polydispersity and the agglomeration of  $\text{Fe}_3\text{O}_4$  nanoparticles. These materials had almost 30–60 % lower saturation magnetization compared to their theoretical values based on the content of  $\text{Fe}_3\text{O}_4$ , resulting in poor magnetic performance. Therefore, tailored methods are needed for in situ dispersion of surface-modified  $\text{Fe}_3\text{O}_4$  nanoparticles to improve their dispersity and uniformity in precursor suspensions.

In recent years, initiation of microdroplet coalescence based on varying velocity gradients and interfacial tension gradients in microchannels has attracted considerable attention. On account of high gradients due to the opposite wettabilities of microchannel walls (for example, a microchannel with a glass plate and a polydimethylsiloxane plate), slip flow forms on one side while regular flow remains on the other side.<sup>33,34</sup> The shift of flow centerline offers high energy for droplet collision and coalescence.<sup>35</sup> This novel strategy based on flow-induced droplet coalescence would be an attractive alternative for preparing nanosuspensions with uniform and monodispersed nanoparticles. Because with the continuous droplet coalescence, numerous hydrophobic particles could be efficiently dispersed into the organic phase as long as they were adequately modified.<sup>36–38</sup> As such, we suggest in situ dispersing surface-modified  $\text{Fe}_3\text{O}_4$  nanoparticles by controlling microdroplet coalescence, and preparing  $\text{Fe}_3\text{O}_4$ /PS composite particles using the  $\text{Fe}_3\text{O}_4$  nanosuspensions.

In this effort, a plate-type microchannel with channel walls of opposite wettabilities was used to direct droplet coalescence and simultaneously disperse surface-modified  $\text{Fe}_3\text{O}_4$  nanoparticles into the oil phase. With the as-prepared  $\text{Fe}_3\text{O}_4$  nanosuspensions, a series of  $\text{Fe}_3\text{O}_4$ /PS composite particles were fabricated via anionic polymerization. The effects of operating conditions were directly examined. Both the  $\text{Fe}_3\text{O}_4$  nanosuspensions and the  $\text{Fe}_3\text{O}_4$ /PS composites were fully characterized to investigate the influence of the dispersion method on particle properties.

## 2. Experimental

### 2.1 Materials

Ferric chloride hexahydrate ( $\text{FeCl}_3 \cdot \text{H}_2\text{O}$ , 99.0 %), ferrous chloride tetrahydrate ( $\text{FeCl}_2 \cdot \text{H}_2\text{O}$ , 99.0 %), potassium persulfate ( $\text{K}_2\text{S}_2\text{O}_8$ , 99.5 %), and aqueous ammonia ( $\text{NH}_3 \cdot \text{H}_2\text{O}$ , 25.0 %) were purchased from Beijing Chemical Works, Co. Cyclohexane (99.5 %), styrene (99.0 %), acetone (99.6 %), and ethanol (99.8 %) were purchased from Tianjin Yongda Chemical Works, Co. The surfactant, alkyl polyglycoside (APG, PG2062, 92.0 %), was purchased from Cognis Co. and used as received.

### 2.2 Apparatus

Fig. 1 illustrates the in situ dispersion route. Two microchannels were used to generate microdroplets and initiate droplet coalescence, respectively. The two plates of the upstream microchannel (Microchannel 1) and the bottom plate of the downstream (Microchannel 2) microchannel were fabricated from PDMS plates using soft lithography technique. To seal the downstream microchannel, the bottom PDMS plate was treated with a solution of sodium-naphthalene and then bonded with a glass plate. Prior to use, the sealed downstream microchannel was washed several times with acetone to ensure that the plate surfaces have reverted to their initial wettabilities.

At the first microchannel, where the upper plate was also made of PDMS, the equal-sized branch channels for dispersed phase flows were 200  $\mu\text{m}$  in width and 200  $\mu\text{m}$  in depth; while the main channel had a width of 400  $\mu\text{m}$ , a depth of 400  $\mu\text{m}$ , and a length of 50 mm. The droplet coalescence was directed by the sudden expansion of the second channel, where the upper plate is made of glass. The expanded section was 2 mm in width and 100 mm in length. A depth of 800  $\mu\text{m}$  was chosen to provide a geometric confinement for initiating microdroplet coalescence.

### 2.3 Preparation of $\text{Fe}_3\text{O}_4$ nanoparticles

The precursor  $\text{Fe}_3\text{O}_4$  suspensions were prepared by a modified coprecipitation method. The mixed aqueous solution of  $\text{FeCl}_3$  and  $\text{FeCl}_2$  with a molar ratio of 2:1 ( $\text{Fe}^{3+}:\text{Fe}^{2+}$ ) served as a dispersed phase flow. APG, whose content was varied based

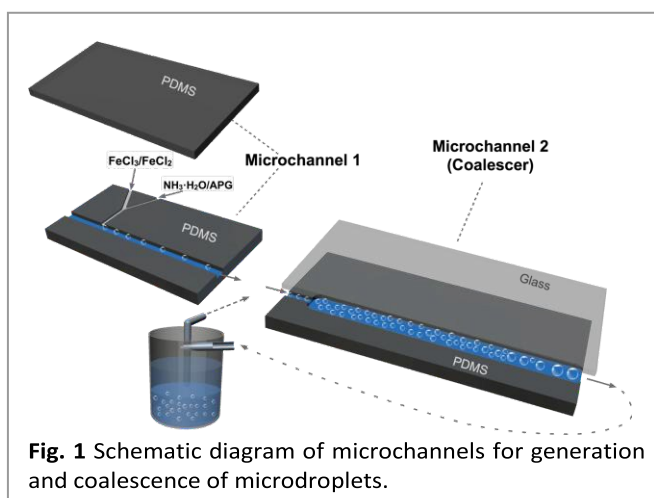


Fig. 1 Schematic diagram of microchannels for generation and coalescence of microdroplets.

on the molar fraction (0–0.0015) of  $\text{Fe}_3\text{O}_4$ , was dissolved in  $\text{NH}_3\cdot\text{H}_2\text{O}$  aqueous solution first. All the solutions were deoxygenated by bubbling  $\text{N}_2$  gas for 2 hours prior to use. In a typical synthesis, the mutually soluble solutions of  $\text{FeCl}_3/\text{FeCl}_2$  (0.12–1.88 mol/L and 0.06–0.94 mol/L) and  $\text{NH}_3\cdot\text{H}_2\text{O}/\text{APG}$  (0.48–7.52 mol/L and 0–0.0014 mol/L) both as the dispersed phase were infused into Microchannel 1 at 50–200  $\mu\text{L}/\text{min}$ . The styrene as the continuous phase was infused at 50–1600  $\mu\text{L}/\text{min}$ . Microdroplets of the aqueous solution were generated in the cross-flowing stream of styrene.  $\text{Fe}_3\text{O}_4$  nanoparticles were synthesized and modified when the two dispersed flows mixed with each other. Downstream, this emulsion was immediately introduced into Microchannel 2 for coalescence. At the outlet of the channel, alternating segments of the emulsion and the styrene phases flowed through the outlet pipe. Collecting the outflow with a volumetric glass vessel, we obtained two separate phases, the limp styrene phase in the upper layer and the emulsion phase in the bottom layer. Then the emulsion was recycled into Microchannel 2 for further demulsification. The circulation was stopped when no decrease in the emulsion volume could be observed. In the end, the styrene-based  $\text{Fe}_3\text{O}_4$  nanosuspensions as the precursor for  $\text{Fe}_3\text{O}_4/\text{PS}$  composites were obtained in the upper layer, while the volume of the bottom layer was greatly reduced.

In a control experiment,  $\text{Fe}_3\text{O}_4$  nanosuspensions were also prepared through subsequent dispersion. In this case, only the upstream microchannel was used, where the  $\text{FeCl}_3/\text{FeCl}_2$  and  $\text{NH}_3\cdot\text{H}_2\text{O}/\text{APG}$  solutions mentioned above (without styrene) were introduced and mixed to synthesize and modify nanoparticles. The suspension was collected right after the mixing process and then was stirred for 30 min. Then the precipitates were separated from the solvent by centrifugation (5000 rpm for 5 min). After the precipitates were washed several times with deionized water and ethanol, surface-modified  $\text{Fe}_3\text{O}_4$  nanoparticles were obtained and then added to styrene at a concentration equal to that of the samples from the in situ dispersion process.

#### 2.4 Preparation of $\text{Fe}_3\text{O}_4/\text{PS}$ composite particles

To prepare  $\text{Fe}_3\text{O}_4/\text{PS}$  composite particles, 20 g styrene-based  $\text{Fe}_3\text{O}_4$  nanosuspensions were dispersed in 65 g cyclohexane according to the method of inverse emulsion polymerization. Prior to use, cyclohexane was bubbled with  $\text{N}_2$  gas under stirring (600 rpm) for 15 min. The polymerization was carried out with  $\text{K}_2\text{S}_2\text{O}_8$  (0.02 g in 10 mL deionized water) as an initiator. The mixture was stirred (600 rpm) for 20 h at 65 °C and  $\text{N}_2$  gas was continuously purged in the flask during this process. After the reaction was completed, the obtained  $\text{Fe}_3\text{O}_4/\text{PS}$  particles were magnetically separated, washed three times with ethanol, and finally vacuum-dried at 60 °C for 12 h.

#### 2.5 Characterization methods

For visualization of droplet coalescence, digital micrographs of the microdroplets were taken using a JEOL-2010 microscope with a high-speed CCD camera (magnifications of 20–200  $\times$ ). Morphologies of  $\text{Fe}_3\text{O}_4/\text{PS}$  composite particles and  $\text{Fe}_3\text{O}_4$  nanoparticles were observed using a scanning electron microscope (SEM; JEOL JSM 7401F) at 10 keV and a transmission electron microscope (TEM; JEOL 100CX) at 100 keV. Dynamic light scattering (DLS) of colloidal  $\text{Fe}_3\text{O}_4$  nanoparticles in suspensions was measured using a Brookhaven BI-200SM laser light scattering spectrometer (semiconductor laser light source, 532 nm). X-ray diffraction (XRD) patterns of  $\text{Fe}_3\text{O}_4$  nanoparticles were measured from  $2\theta$  of 20°–70° (Rigaku Corporation D/max-RB). Contact angles of  $\text{Fe}_3\text{O}_4$  nanoparticles were measured using an optical drop shape analyzer (DataPhysics SCA20).  $\text{Fe}_3\text{O}_4$  content in  $\text{Fe}_3\text{O}_4/\text{PS}$  composites was determined by thermogravimetric analysis (TGA; STA 409 PC). Magnetic hysteresis loops of  $\text{Fe}_3\text{O}_4/\text{PS}$  composites were measured by a XL-7 model magnetic property measurement system (MPMS; Quantum Design) at 20 °C. 1 g of the dried  $\text{Fe}_3\text{O}_4/\text{PS}$  composites were compacted and placed in the circuit, where DC (direct current) was used. By gradually increasing the exciting current to change the magnetic field, hysteresis loop was measured by numerical integration.

### 3. Results and discussion

To quantify the influence of microdroplet coalescence on the in situ dispersion of surface-modified  $\text{Fe}_3\text{O}_4$  nanoparticles, operating conditions were systemically investigated. To this end, both the coalescence and the particle transfer efficiencies were assessed first.  $\text{Fe}_3\text{O}_4/\text{PS}$  composite particles were then fabricated from the styrene-based  $\text{Fe}_3\text{O}_4$  suspensions to assess the crucial role of the precursor.

#### 3.1 Microdroplet coalescence and in situ dispersion

The efficiencies of microdroplet coalescence and in situ dispersion of surface-modified nanoparticles are defined to account for their relationship. The coalescence efficiency ( $E_c$ ) can be calculated by the following equation:

$$E_c = \frac{V_{\text{upper}}}{V_{\text{oil}}} \times 100\% \quad (1)$$

where  $V_{\text{upper}}$  is the volume of the upper layer in the vessel and  $V_{\text{oil}}$  is the total volume of the styrene used in the preparation experiment. The dispersion efficiency ( $E_T$ ) of the surface-modified nanoparticles, which can also be regarded as the phase transfer efficiency, is obtained by measuring the solid content of the upper layer:

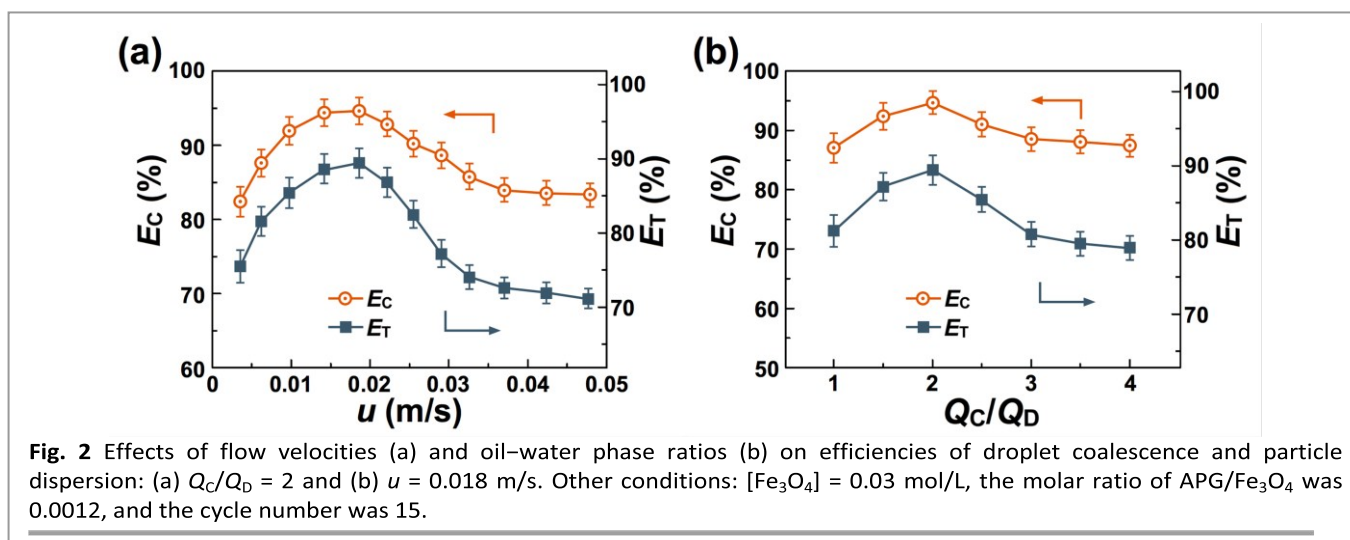


**Fig. 2** Effects of flow velocities (a) and oil–water phase ratios (b) on efficiencies of droplet coalescence and particle dispersion: (a)  $Q_C/Q_D = 2$  and (b)  $u = 0.018$  m/s. Other conditions:  $[\text{Fe}_3\text{O}_4] = 0.03$  mol/L, the molar ratio of APG/ $\text{Fe}_3\text{O}_4$  was 0.0012, and the cycle number was 15.

$$E_T = \frac{m_{\text{upper}}}{m_{\text{particle}}} \times 100\% \quad (2)$$

where  $m_{\text{upper}}$  is the mass of particles in the upper layer and  $m_{\text{particle}}$  is the total mass of modified particles.

The efficiencies of microdroplet coalescence and particle dispersion at varying flow velocities are presented in Fig. 2a.  $E_T$  was simultaneously enhanced by the droplet coalescence and exhibited the same trend as  $E_C$  with the increasing flow velocity. A higher flow velocity increased collision probability of microdroplets due to the increasing intensity of slip flow, which changed the flow direction of the droplets and drove them to collide and coalesce. With the continuous increase in the flow velocity, although slip flow was intense and favorable for droplet coalescence, the residence time (defined as the total length of both the channels divided by the flow velocity) was shortened and the collision frequency of the droplets was simultaneously decreased. Under optimal conditions,  $E_C$  and  $E_T$  were as high as 94 % and 89 %, respectively.

Analysis of the effect of oil–water phase ratio ( $Q_C/Q_D$ ) on the coalescence and dispersion efficiencies is presented in Fig. 2b.  $E_C$  and  $E_T$  first increased dramatically to 94 % and 89 % at  $Q_C/Q_D = 2$ . Thereafter, they gradually decreased at  $Q_C/Q_D$  above 2. The results indicate that at lower ratios, numerous

hydrophobic nanoparticles tended to assemble in the superficial layer of styrene and stabilize the microdroplets, giving rise to the decrease in  $E_C$  and  $E_T$ . With the increase in the collision distance due to high phase ratios, droplet coalescence was correspondingly reduced and the mass transfer of hydrophobic  $\text{Fe}_3\text{O}_4$  nanoparticles into the oil phase seemed to be inhibited.

Particle concentration is an important operating parameter in a dispersion process. A high concentration often causes nanoparticles to assemble at interfaces, which inhibits the particle dispersion. The results presented in Fig. 3a show the influence of particle concentration (in terms of molar amounts of particles in oil phase) on  $E_C$  and  $E_T$ . As the concentration increased, both  $E_C$  and  $E_T$  decreased gradually. It should be noted, however, that even at a high concentration of 0.47 mol/L,  $E_C$  and  $E_T$  were still approximately 87 % and 82 % of their initial values, respectively. These results imply a relatively high efficiency of particle dispersion by microdroplet coalescence, even at high concentrations when hydrophobic nanoparticles could stabilize water-in-oil emulsions and inhibit coalescence.

Fig. 3b shows the variations of  $E_C$  and  $E_T$  with respect to particle hydrophobicities (in the form of contact angle, as

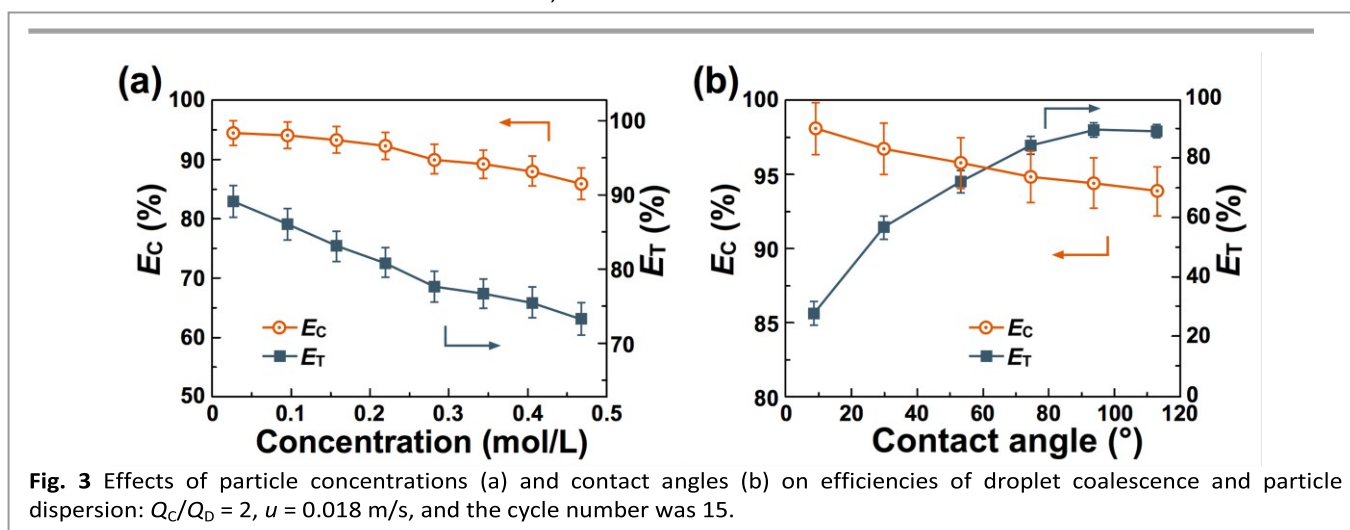


**Fig. 3** Effects of particle concentrations (a) and contact angles (b) on efficiencies of droplet coalescence and particle dispersion:  $Q_C/Q_D = 2$ ,  $u = 0.018$  m/s, and the cycle number was 15.

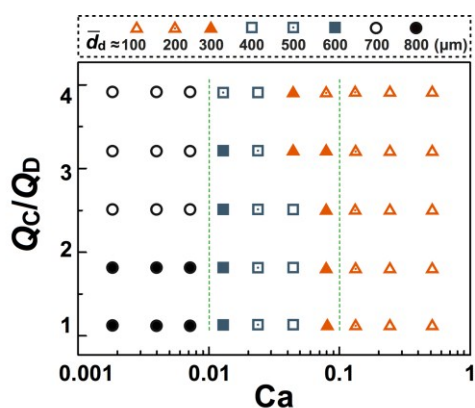
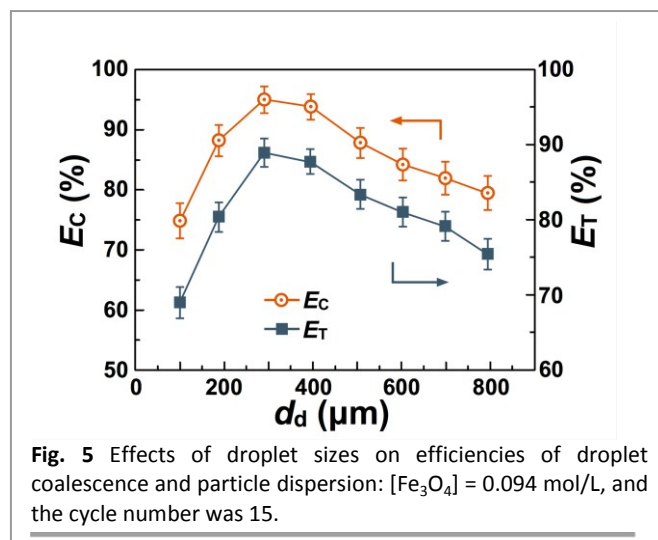
**Table 1** Corresponding characteristic parameters of APG-modified  $\text{Fe}_3\text{O}_4$  nanoparticles.

Sample	1	2	3	4	5	6
Contact angle ( $^\circ$ )	8.8	29.6	53.0	74.5	93.2	112.8
Molar ratio of APG to $\text{Fe}_3\text{O}_4$	0	0.0003	0.0006	0.0009	0.0012	0.0015

listed in Table 1). With the increase in particle hydrophobicity, opposite trends between  $E_C$  and  $E_T$  were observed: an expected increase in dispersion efficiency along with a slightly decreased coalescence efficiency, which should be attributed to the stabilizing effect of hydrophobic particles on w/o emulsions. Nevertheless, the dispersion of nanoparticles in the w/o emulsion system should be performed on the premise of surface modification of a certain degree. The additive content of the surfactant was determined to be 0.0012:1 (a molar ratio of APG to  $\text{Fe}_3\text{O}_4$ ).

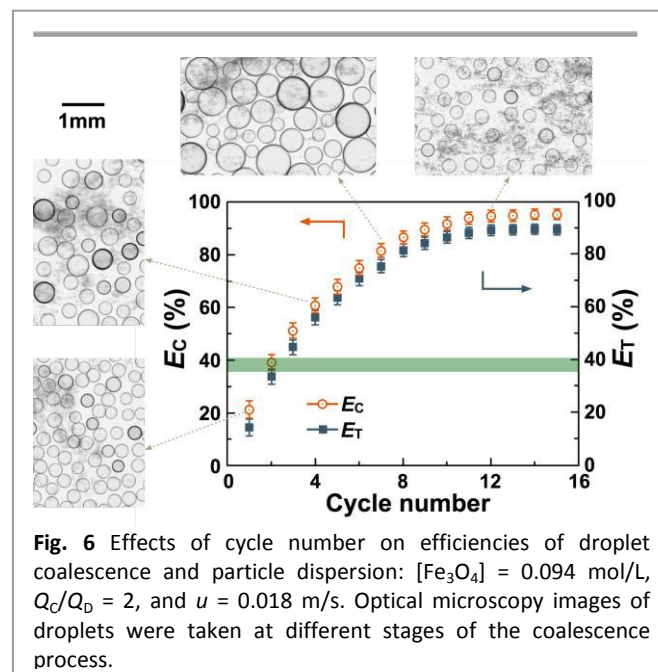
Since the initial droplet size has a great influence on the coalescence process, the range of phase ratio ( $Q_C/Q_D$ ) and capillary number ( $Ca$ ,  $Ca = u\mu/\gamma$ ) of the continuous phase (in the downstream channel) should be identified according to droplet size, as shown in Fig. 4. This graph can be divided into three regions:  $Ca < 0.001$ ,  $0.001 < Ca < 0.01$ , and  $Ca > 0.1$ , according to the different parameters that are dominant in droplet size:  $Q_C/Q_D$ , both  $Q_C/Q_D$  and  $Ca$ , and  $Ca$ , respectively.  $Q_C/Q_D$  can change the intensity of slip flow by varying the distance between droplets and channel walls; while  $Ca$  represents the shear force that exerts efforts on droplet collision. At  $Ca < 0.01$ , the droplet size was mainly determined by the physical properties of the system. With the increase in  $Ca$  ( $0.01 < Ca < 0.1$ ), the shear force dominated the process. As a result, the droplet size was simultaneously increased with  $Ca$  and  $Q_C/Q_D$ . Emulsions with the smallest droplets (50–100  $\mu\text{m}$ ) were found at a higher  $Ca$  ( $Ca > 0.1$ ) where the influence of phase ratio was negligible.

On the basis of the droplet size division as a function of

**Fig. 4** Operating diagram organizing droplet behavior as a function of capillary number and phase ratio:  $[\text{Fe}_3\text{O}_4] = 0.094 \text{ mol/L}$ , and symbols denote average droplet sizes. The cycle number was 15.**Fig. 5** Effects of droplet sizes on efficiencies of droplet coalescence and particle dispersion:  $[\text{Fe}_3\text{O}_4] = 0.094 \text{ mol/L}$ , and the cycle number was 15.

phase ratio and  $Ca$ , the effects of initial droplet size on in situ dispersion were also investigated (Fig. 5). As observed at a variety of initial droplet sizes (monodispersed with polydispersity indexes of 0.039–0.048, Table S1), both the efficiencies of droplet coalescence and particle dispersion reached the maximum values at sizes of 200–300  $\mu\text{m}$ , corresponding to the process at  $Q_C/Q_D$  of 2 and  $Ca$  of 0.16–0.18. In this process, large droplets are favorable for coalescence owing to their high flexibility; while elastic collision tends to occur for the small droplets even at intense slip flow conditions, hindering both the microdroplet coalescence and particle dispersion processes.

Circulation experiments were conducted to measure the efficiencies of droplet coalescence and particle dispersion. The results are shown in Fig. 6, where the green region represents the dispersion efficiency of the subsequent dispersion for comparison. As observed during the process, both  $E_C$  and  $E_T$  increased sharply as the cycle number increased and leveled

**Fig. 6** Effects of cycle number on efficiencies of droplet coalescence and particle dispersion:  $[\text{Fe}_3\text{O}_4] = 0.094 \text{ mol/L}$ ,  $Q_C/Q_D = 2$ , and  $u = 0.018 \text{ m/s}$ . Optical microscopy images of droplets were taken at different stages of the coalescence process.

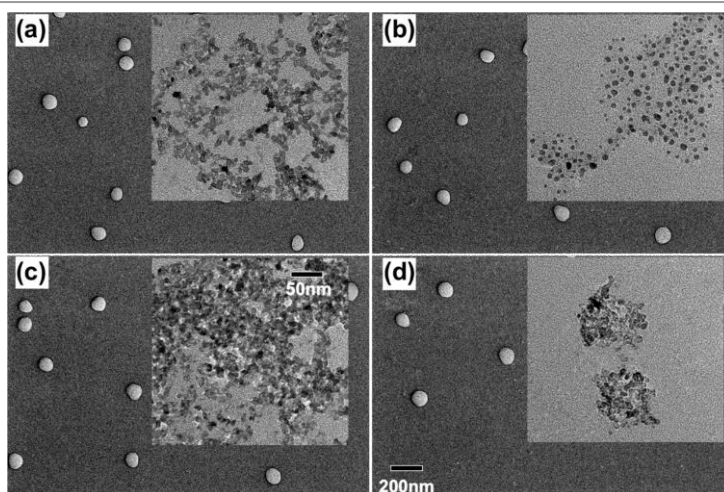


**Fig. 7** TEM images of  $\text{Fe}_3\text{O}_4$  nanoparticles and SEM images of  $\text{Fe}_3\text{O}_4/\text{PS}$  composites obtained through different processes: (a) in situ dispersion,  $[\text{Fe}_3\text{O}_4] = 0.47$  mol/L; (b) in situ dispersion,  $[\text{Fe}_3\text{O}_4] = 0.094$  mol/L; (c) subsequent dispersion,  $[\text{Fe}_3\text{O}_4] = 0.47$  mol/L; (d) subsequent dispersion,  $[\text{Fe}_3\text{O}_4] = 0.094$  mol/L. Other conditions for (a) and (c):  $Q_C/Q_D = 2$ , and  $u = 0.018$  m/s.

off to approximately 94 % and 89 % within 12 times, which should be attributed to the timely removal of hydrophobic nanoparticles at phase interfaces. By contrast,  $E_T$  of the subsequent dispersion could only reach a value of 36–41 %. Therefore, the resistance of particle gathering to dispersion was considered to be overcome owing to the intensification by directing microdroplet coalescence. The coalescing microstructures also progressed during circulation, illustrated by the micrographs of microdroplets (Fig. 6). The droplets, which were initially uniform in size, exhibited varying size with the continuous circulation. At the first 4 cycles, the droplet size increased significantly due to the coalescence and reached the highest value of approximately 810  $\mu\text{m}$ . Afterwards, the size decreased sharply and the droplets were even smaller than the initial droplets, suggesting that larger droplets had coalesced and been separated from the emulsion.

### 3.2 Characterization of $\text{Fe}_3\text{O}_4$ nanocolloids and composite particles

SEM images of the  $\text{Fe}_3\text{O}_4/\text{PS}$  composite particles prepared using different precursor suspensions are shown in Fig. 7, where TEM images of raw  $\text{Fe}_3\text{O}_4$  nanoparticles are also exhibited in corresponding panels. For the composites, there exists little difference among all the samples. The composite particles have almost the same morphology and are uniform in size. However, their precursor suspension contained surface-modified  $\text{Fe}_3\text{O}_4$  nanoparticles with large differences. In the case of subsequent dispersion, the samples (Figs. 7c and 7d) were composed of agglomerated nanoparticles, which were unfavorable for magnetic performance. Even at a lower concentration of 0.094 mol/L, the nanoparticles were still agglomerated. By contrast, upon in situ dispersion, monodispersed  $\text{Fe}_3\text{O}_4$  nanoparticles could be controllably prepared (Figs. 7a and 7b). Even at 0.47 mol/L (Fig. 7a), the particles were basically monodispersed and similar in size. The reason should be attributed to the fact that small nanoparticles were rapidly transferred into the organic phase,

so that nanoparticle growth and agglomeration could be suppressed.

In addition, the  $\text{Fe}_3\text{O}_4$  nanoparticles in suspensions were also investigated by DLS to determine the colloidal size distribution, as shown in Fig. 8. The DLS results of all the samples show a single population with an average size of  $13 \pm 3$  nm. As expected, the average size of the nanoparticles obtained through in situ dispersion was smaller than that of the samples from subsequent dispersion at the same concentrations. Especially for the sample at the higher concentration of 0.47 mol/L (Fig. 8d), the DLS data were skewed to higher sizes and the distribution became wider due to nanoparticle agglomeration, which was consistent with the TEM results.

X-ray diffraction patterns of the prepared  $\text{Fe}_3\text{O}_4$

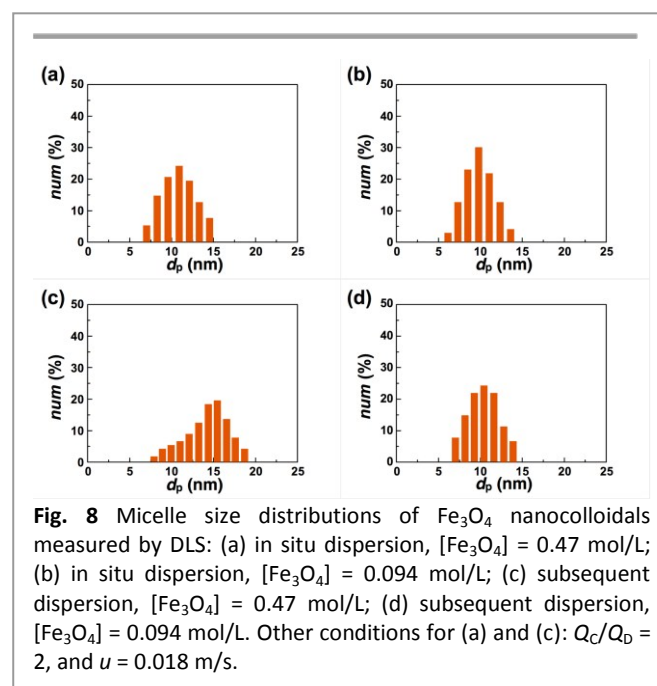
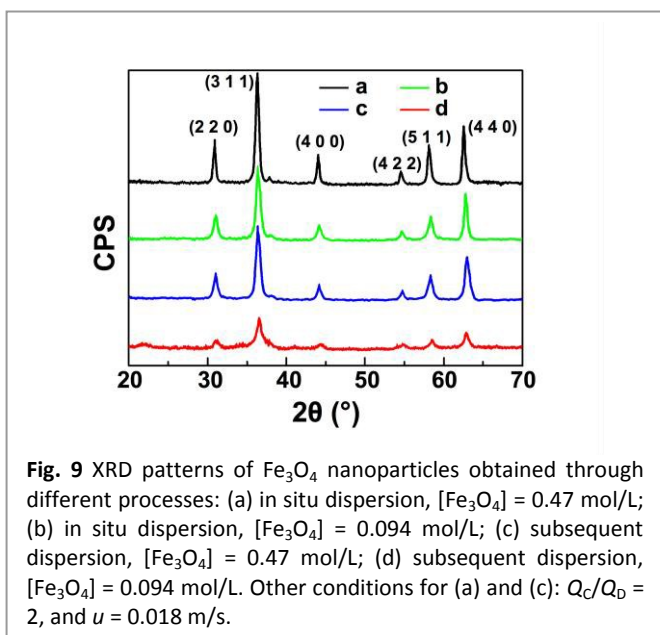


**Fig. 8** Micelle size distributions of  $\text{Fe}_3\text{O}_4$  nanocolloids measured by DLS: (a) in situ dispersion,  $[\text{Fe}_3\text{O}_4] = 0.47$  mol/L; (b) in situ dispersion,  $[\text{Fe}_3\text{O}_4] = 0.094$  mol/L; (c) subsequent dispersion,  $[\text{Fe}_3\text{O}_4] = 0.47$  mol/L; (d) subsequent dispersion,  $[\text{Fe}_3\text{O}_4] = 0.094$  mol/L. Other conditions for (a) and (c):  $Q_C/Q_D = 2$ , and  $u = 0.018$  m/s.

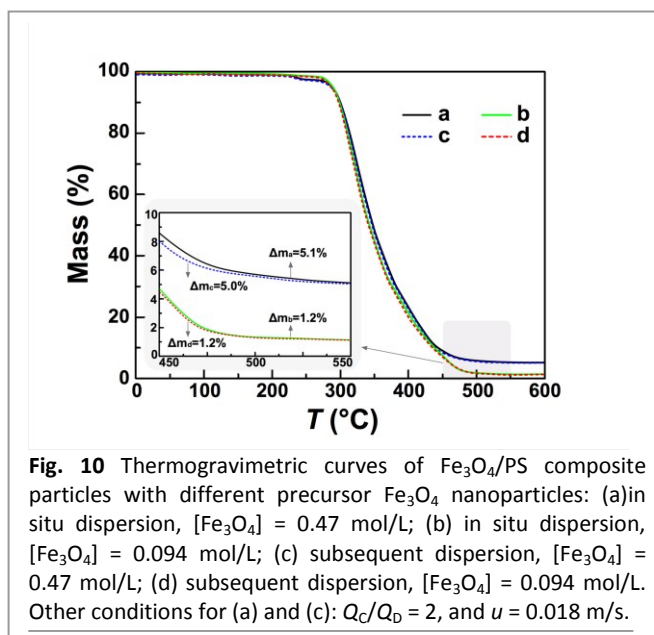


nanoparticles are shown in Fig. 9. The samples were also sampled from the suspensions of 0.094 mol/L and 0.47 mol/L through both the in situ and the subsequent dispersion methods, respectively. All the nanoparticles are primarily of face-centered magnetite  $\text{Fe}_3\text{O}_4$  crystalline phase, as evident from comparison of the diffraction peaks to the JCPDS database (No. 79-0418). The characteristic peaks are all observed in the XRD patterns at  $2\theta$  of  $30.1^\circ$ ,  $35.5^\circ$ ,  $43.1^\circ$ ,  $53.4^\circ$ ,  $57.0^\circ$ , and  $62.6^\circ$  corresponding to the diffractions of (2 2 0), (3 1 1), (4 0 0), (4 2 2), (5 1 1), and (4 4 0) planes. As seen in the XRD patterns, face-centered magnetite  $\text{Fe}_3\text{O}_4$  crystalline phase is clearly present as the main phase. Nevertheless, for the case of in situ dispersion, the phase intensity was slightly increased.

### 3.3 Magnetic properties of $\text{Fe}_3\text{O}_4/\text{PS}$ composite particles

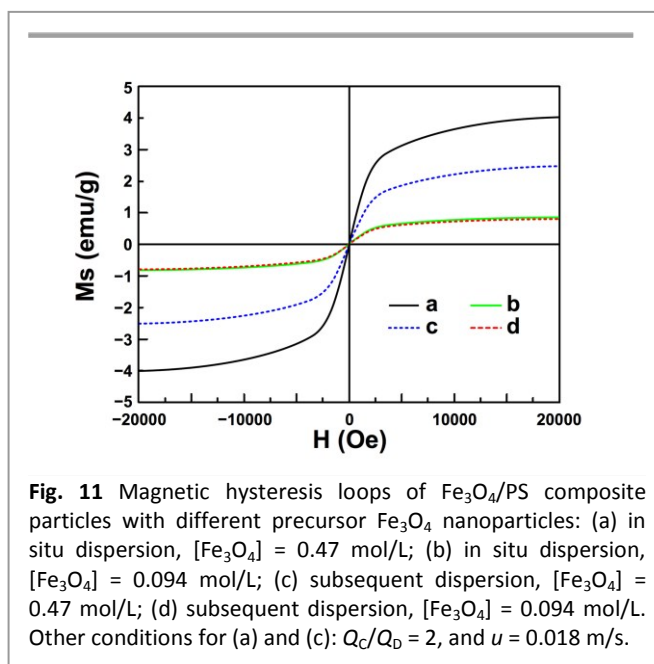
To determine the mass percentage of  $\text{Fe}_3\text{O}_4$  in  $\text{Fe}_3\text{O}_4/\text{PS}$  composite particles, a set of TGA experiments was conducted for each sample, as shown in Fig. 10. One can see that during the experiments, the mass of  $\text{Fe}_3\text{O}_4$  in all the samples could be described by a slow decrease at  $235\text{--}270^\circ\text{C}$  (decomposition of APG), followed by a fast mass loss at temperatures ranging from  $280$  to  $510^\circ\text{C}$  (decomposition of PS). At temperatures above  $550^\circ\text{C}$ , PS was completely decomposed. The accurate residual mass should be attributed to  $\text{Fe}_3\text{O}_4$ , which was the basis of comparison of magnetic performance. According to the TGA results, the magnetite ( $\text{Fe}_3\text{O}_4$ ) content of the composites was evaluated to be 5.1 wt %, 5.0 wt %, 1.2 wt %, and 1.2 wt %, respectively.

Decreasing magnetite nanoparticle size is favorable for enhancing superparamagnetic performance and reducing ferrimagnetic performance at the same time. As were expected from the control of particle size in the range of below 20 nm, all the samples exhibited zero coercivity and remanence in hysteresis loops (Fig. 11), which was in accordance with the superparamagnetic behavior. Additionally, the saturation magnetizations of  $\text{Fe}_3\text{O}_4/\text{PS}$  composites were



found to be 0.816 emu/g at 1.2 wt % for both the samples (curves b and d in Fig. 11). In comparison to the concentration of 0.47 mol/L, the saturation magnetization of the sample prepared using in situ dispersed  $\text{Fe}_3\text{O}_4$  nanoparticles was up to 4.012 emu/g (the theoretical maximum for the saturation magnetization of composite  $\text{Fe}_3\text{O}_4$  is 4.25 emu/g at 5 wt %), approximately 56 % larger than that of the sample with the subsequently dispersed  $\text{Fe}_3\text{O}_4$  nanoparticles (curves a and c in Fig. 11). Even compared with the saturation magnetization of  $\text{Fe}_3\text{O}_4$  composites in other studies, it is still 15–30 % larger at a magnetic content of around 5 wt % (whose saturation magnetizations were 2.8–3.5 emu/g).<sup>21,25,26</sup> This result clearly confirms that the monodispersity of raw  $\text{Fe}_3\text{O}_4$  nanoparticles, which could be increased by in situ dispersion, plays a key role in the magnetic performance of  $\text{Fe}_3\text{O}_4$ -based composites.

In brief, the enhancement of magnetic performance of



Fe<sub>3</sub>O<sub>4</sub>/PS composites by preparing with in situ dispersed Fe<sub>3</sub>O<sub>4</sub> nanoparticles was preliminarily confirmed. The flow-induced droplet coalescence remarkably improved the nanoparticle dispersion behavior. In this case, the monodispersity, size, and size uniformity of the surface-modified Fe<sub>3</sub>O<sub>4</sub> nanoparticles have also benefited from timely removal of interfacial nanoparticles during the preparation. However, the preparation of nanosuspensions via in situ dispersion requires further research because the particle concentration still needs considerably increasing, especially for applications in the preparation of composite materials with high-content inorganic nanoparticles.

#### 4. Conclusions

A method for in situ dispersion of surface-modified Fe<sub>3</sub>O<sub>4</sub> nanoparticles by controlling microdroplet coalescence has been developed in this study. The droplet coalescence was successfully performed in the plate-type microchannel. Monodispersed and uniformly distributed Fe<sub>3</sub>O<sub>4</sub> nanoparticles with an average size of approximately 12 nm could be controllably prepared due to timely removal of surface-modified nanoparticles into organic phase. By virtue of high-quality precursors, the resulting Fe<sub>3</sub>O<sub>4</sub>/PS composite particles exhibit superparamagnetic behaviors, with a saturation magnetization of up to 4.012 emu/g at the magnetite content of 5 wt %. The experimental result also confirms that the monodispersity of the raw magnetite nanoparticles plays a key role in the magnetic performance of Fe<sub>3</sub>O<sub>4</sub> composites.

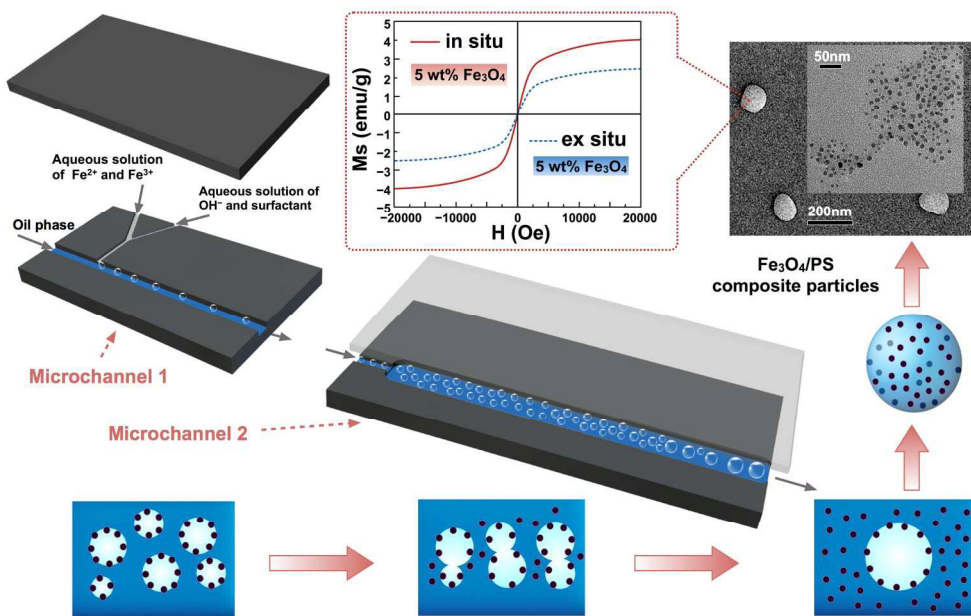
Although more systematic studies are needed, this method still has great potential to be tailored to the preparation of high-quality nanosuspensions for downstream processes. Future studies should focus on increasing the particle concentration of nanosuspensions and corresponding mechanisms of particle movement during the in situ dispersion process.

#### Acknowledgements

We gratefully acknowledge the support of the National Basic Research Foundation of China (Grant No. 2013CB733600), the National Natural Science Foundation of China (91334201, 21036002, 21276140, 21506004), and the Fundamental Research Funds for the Central Universities of China (ZY1630).

#### References

- 1 Y.-H. Lai, M.-H. Hsu and J.-T. Yang, *Lab. Chip.*, 2010, **10**, 3149–3156.
- 2 L. Isa, E. Amstad, K. Schwenke, E. Del Gado, P. Ilg, M. Kroeger and E. Reimhult, *Soft Matter*, 2011, **7**, 7663–7675.
- 3 C. C. Chan and Y. C. Chen, *Sep. Sci. Technol.*, 2002, **37**, 3407–3420.
- 4 C. Cornelus, M. P. Krafft and J. G. Riess, *Artif. Cell Blood Sub.*, 1994, **22**, 1267–1272.
- 5 R. J. de Korte, J. C. Schouten and C. M. van den Bleek, *AIChE J.*, 2001, **47**, 851–860.
- 6 H. Feng, D. Ershov, T. Krebs, K. Schroen, M. A. C. Stuart, J. van der Gucht and J. Sprakel, *Lab. Chip.*, 2015, **15**, 188–194.
- 7 R. D. Narhe, M. D. Khandkar, K. P. Adhi, A. V. Limaye, S. R. Sainkar and S. B. Ogale, *Phys. Rev. Lett.*, 2001, **86**, 1570–1573.
- 8 J. Yan, J. Liu, P. Jing, C. Xu, J. Wu, D. Gao and Y. Fang, *Soft Matter*, 2012, **8**, 11697–11703.
- 9 K. Wang, Y. Lu, L. Yang and G. Luo, *AIChE J.*, 2013, **59**, 643–649.
- 10 S. Kredentser, O. Buluy, P. Davidson, I. Dozov, S. Malynych, V. Reshetnyak, K. Slyusarenko and Y. Reznikov, *Soft Matter*, 2013, **9**, 5061–5066.
- 11 N. Bremond, A. R. Thiam and J. Bibette, *Phys. Rev. Lett.*, 2008, **100**, 024501.
- 12 J. Shemesh, A. Nir, A. Bransky and S. Levenberg, *Lab. Chip.*, 2011, **11**, 3225–3230.
- 13 H. Tokumitsu, H. Ichikawa and Y. Fukumori, *Pharmaceut. Res.*, 1999, **16**, 1830–1835.
- 14 C. Verdier and M. Brizard, *Rheol. Acta*, 2002, **41**, 514–523.
- 15 D. I. Tee, M. Mariatti, A. Azizan, C. H. See and K. F. Chong, *Compos. Sci. Technol.*, 2007, **67**, 2584–2591.
- 16 G. F. Christopher, J. Bergstein, N. B. End, M. Poon, C. Nguyen and S. L. Anna, *Lab. Chip.*, 2009, **9**, 1102–1109.
- 17 H. Tan, Y. Lin, J. Zheng, J. Gong, J. Qiu, H. Xing and T. Tang, *Soft Matter*, 2015, **11**, 3986–3993.
- 18 B. Carlberg, L.-L. Ye and J. Liu, *Small*, 2011, **7**, 3057–3066.
- 19 K. Shimba, K. Furuta, N. Morimoto, N. Tezuka and S. Sugimoto, *Mater. Trans.*, 2011, **52**, 486–490.
- 20 S. Reinicke, S. Doehler, S. Tea, M. Krekhova, R. Messing, A. M. Schmidt and H. Schmalz, *Soft Matter*, 2010, **6**, 2760–2773.
- 21 J. Luis Miettä, P. I. Tamborenea and R. Martin Negri, *Soft Matter*, 2016, **12**, 422–431.
- 22 F.-H. Chen, L.-M. Zhang, Q.-T. Chen, Y. Zhang and Z.-J. Zhang, *Chem. Commun.*, 2010, **46**, 8633–8635.
- 23 Y. Chen, B. Song, L. Lu and J. Xue, *Nanoscale*, 2013, **5**, 6797–6803.
- 24 C. Stefaniu, M. Chanana, H. Ahrens, D. Wang, G. Brezesinski and H. Moehwald, *Soft Matter*, 2011, **7**, 4267–4275.
- 25 B. Zhao and Z. Nan, *Nanoscale Res. Lett.*, 2011, **6**, 230.
- 26 A. S. Semisalova, N. S. Perov, G. V. Stepanov, E. Y. Kramarenko and A. R. Khokhlov, *Soft Matter*, 2013, **9**, 11318–11324.
- 27 W. Jiao, M. Shioya, R. Wang, F. Yang, L. Hao, Y. Niu, W. Liu, L. Zheng, F. Yuan, L. Wan and X. He, *Compos. Sci. Technol.*, 2014, **99**, 124–130.
- 28 R. Y. Hong, B. Feng, G. Liu, S. Wang, H. Z. Li, J. M. Ding, Y. Zheng and D. G. Wei, *J. Alloys Compd.*, 2009, **476**, 612–618.
- 29 Y. Chen, Z. Qian and Z. Zhang, *Colloid Surface. A*, 2008, **312**, 209–213.
- 30 Y. Li, D. Chen, X. Liu, Y. Zhou, Q. Zhuang, R. Cai and K. Zhang, *Compos. Sci. Technol.*, 2014, **100**, 212–219.
- 31 A. Ruditskiy, B. Ren and I. Kretzschmar, *Soft Matter*, 2013, **9**, 9174–9181.
- 32 L. Zhou, G. Li, T. An and Y. Li, *Res. Chem. Intermediat*, 2010, **36**, 277–288.
- 33 Y. Okubo, M. Toma, H. Ueda, T. Maki and K. Mae, *Chem. Eng. J.*, 2004, **101**, 39–48.
- 34 X. Chen, H. Lu, W. Jiang, L. Y. Chu and B. Liang, *Ind. Eng. Chem. Res.*, 2010, **49**, 9279–9288.
- 35 R. Deng, D. Y. Arifin, Y. C. Mak and C.-H. Wang, *AIChE J.*, 2009, **55**, 3056–3065.
- 36 X. Mao, G. C. Rutledge and T. A. Hatton, *Langmuir*, 2013, **29**, 9626–9634.
- 37 E. P. Chang and T. A. Hatton, *Langmuir*, 2012, **28**, 9748–9758.
- 38 Q. Q. Zhou, Y. Sun, S. T. Yi, K. Wang and G. S. Luo, *Soft Matter*, 2016, **12**, 1674–1682.



205x127mm (300 x 300 DPI)